

# Titanium uptake and incorporation into silica nanostructures by the diatom *Pinnularia* sp. (Bacillariophyceae)

Matilde Skogen Chauton · Lotte M. B. Skolem ·  
Lasse Mork Olsen · Per Erik Vullum · John Walmsley ·  
Olav Vadstein

Received: 3 June 2014 / Revised and accepted: 3 July 2014 / Published online: 24 July 2014  
© The Author(s) 2014. This article is published with open access at Springerlink.com

**Abstract** Diatoms are an ecologically successful group within the phytoplankton, and their special feature is a biofabricated silica cell encasement called a frustule. These frustules attract interest in material technology, and one potential application is to use them in solar cell technology. The silica frustule with its nanoscaled pattern is interesting per se, but the utility is enhanced if we succeed in incorporating other elements. Titanium is an interesting element because its oxide is a semi-conductor with a high band gap. However, doping with relevant elements through bioincorporation is challenging, and it is necessary to understand the biology involved in element uptake and incorporation. Here we present data on bioincorporation of Ti into the silica frustules of the pennate diatom *Pinnularia* sp. (Ehrenberg) and show that the distribution of the incorporated Ti is inhomogeneous both between and within valves. More than a tenfold increase of Ti in newly synthesised valves was achieved, and increased Ti around the pores was confirmed by both EDS and EELS analyses. HAADF STEM spectroscopy revealed a grainy surface with amorphous silica particles of 4 to 5 nm in size. These observations are explained by what is known from the physico-chemical processes involved in biosilification and frustule formation, looking into it from a biological point of view.

**Keywords** Silica · Titanium · Diatom · Bioincorporation · Frustule · Nanostructure

M. S. Chauton (✉) · L. M. B. Skolem · L. M. Olsen · O. Vadstein  
Department of Biotechnology, Norwegian University of Science and  
Technology (NTNU), SemSeland's veg 6/8, 7491 Trondheim,  
Norway  
e-mail: matilde.chauton@nt.ntnu.no

P. E. Vullum · J. Walmsley  
SINTEF Materials and Chemistry, Postboks 4760 Sluppen,  
7465 Trondheim, Norway

## Introduction

Diatoms possess a cell encasement called the frustule, made of amorphous (i.e. non-crystalline) silica. The frustule consists of two valves, ornamented with species-specific patterns of pores and ribs on meso- and nanoscale dimensions. When the diatom cell divides each new cell will retain one old valve and synthesise one new valve. The actual role of the frustule remains a topic for discussion, but possible functions are light transmission, nutrient transport, gas exchange and grazer or virus protection. Amorphous silica is in principle transparent to visible light (which the living diatom use for photochemical energy synthesis), and it is suggested that the pore pattern provides a photonic crystal function that results in light focusing and transport into the chloroplasts (Yamanaka et al. 2008; De Stefano et al. 2009; Sclafani et al. 2013).

When diatoms grow exponentially (i.e. resource-unlimited growth), silicic acid ( $\text{SiOH}_4$ ) is actively transported via silica transporters (SITs) into the cytoplasm and then via transport vesicles into silica deposition vesicles (SDVs) (Annenkov et al. 2013). This process involves active transport against a concentration gradient from cytosol into the SDV and a pH gradient because the inside of the SDV has a lower pH. In the SDV, silicon (Si) polymerizes to silica ( $\text{SiO}_2$ ), and small building blocks are created. Exactly how these polymers are combined to form a frustule remains unknown (Del Amo and Brzezinski 1999; Zurzolo and Bowler 2001). Frustule construction is most probably a combination of genetically expressed Si transporter proteins that are involved in the transport of Si into the cell (Thamatrakoln and Hildebrand 2007) and post-translationally modified peptides (silaffins, silacidins) and long-chained polyamines involved in Si polymerization and construction of the frustule (Mock et al. 2008; Spinde et al. 2011); Kinrade et al. (2002) observed a transient organosilicon complex in the diatom *Navicula pelliculosa*: hexavalent Si was coordinated to nitrogen, but it was not

possible to determine the localization of these complexes or if they were involved in frustule synthesis.

The highly modifiable frustule surface properties has been exploited in drug delivery technology (Aw et al. 2012), and the mesoporous frustule material has been applied as photocatalyst templates (Mao et al. 2014; He et al. 2013). The use of biogenic Si from diatoms in solar cell technology has been suggested, and the idea is extended to use the intact frustule itself and take advantage of the nanoscaled patterns of pores and rib structures (Jeffryes et al. 2011; Toster et al. 2013). The concentration of Si in aquatic environments is many times higher than other comparable elements, and the frustule composition likely reflects the availability of Si and also other elements: for example, the concentration of anions such as phosphorus is quite high in the frustules possibly because it plays a role in the formation of Si nanoparticles during frustule synthesis (Hildebrand 2008). From a material point of view, on the other hand, there are other elements such as in the semi-conductor TiO<sub>2</sub> that would enhance the functionality of the frustule.

Increased concentrations of functional elements can be achieved by metabolic doping in living cells or by post-modifications such as thermal annealing. TiO<sub>2</sub> (Jeffryes et al. 2008; Lang et al. 2013) and GeO<sub>2</sub> (Gale et al. 2011) have been incorporated by bio-uptake or deposited on the frustules post-cleaning. GeO<sub>2</sub> has been shown to inhibit diatom growth (Shea and Chopin 2007) and to interfere with frustule synthesis (Basharina et al. 2012). The uptake of other elements may be regulated as a function of concentrations, and there will be biological limits to the amount of a specific element that can be incorporated. Ti is not considered an essential element to organisms, but it has been discussed whether this is due to the fact that it is readily available, so we fail to detect its essentiality, or if it is truly non-essential. It is, however, bioactive (Buettner and Valentine 2012), and another consideration when trying to understand biogenic incorporation of various elements into the silica frustule is the potential harmful effects of, for example, TiO<sub>2</sub> nanoparticles. The semi-conductive properties of TiO<sub>2</sub> nanoparticles is desired in solar cells, but in living cells they are toxic in combination with UV light because the nanoparticles can lead to the formation of ROS (Miller et al. 2012). However, microalgae have a naturally high antioxidant protection because of their photosynthetic activity and concurrent oxygen formation. With the emerging field of nanomaterials, it has been shown that nanoparticles can accumulate in organelles such as the mitochondria and disrupt the electron transport chain with increased production of superoxide radicals (Li et al. 2003). It is therefore natural to assume that the uptake and transport of Ti into live cells is a controlled process in some way, where the Ti is directed to cell compartments where it is not damaging, e.g. the SDVs. No specialized Ti uptake or deposition proteins are known for diatoms, but mineralization

of TiO<sub>2</sub> by recombinant silaffins or silicateins has been demonstrated (Sumerel et al. 2003; Cole et al. 2006; Kroger et al. 2006).

Here we present data on uptake and incorporation of Ti in frustules of *Pinnularia* sp. (Ehrenberg), and we show that the photophysiology of *Pinnularia* cells was not adversely affected by the experimental setup and that Ti concentration is strongly enhanced in certain parts of the newly formed valves. Our work is a follow-up of Jeffryes et al. (2008) as we address some points raised in their discussion, in addition to providing new data on SiO<sub>2</sub> particle size and the variability of Ti measurements. Our observations are interpreted in light of what is known about element uptake and deposition in living cells, and we discuss how this knowledge can be used to better understand both the biological function of a frustule and how to modify the frustule as a functional material.

## Materials and methods

### Cultivation, photophysiology and biomass

*Pinnularia* sp. (UTEX B679) was grown in filtered, autoclaved seawater amended with nutrients according to Guillard's f/2-recipe for all elements except Si, which was reduced to 50 %. The natural seawater used here contains around 4 μM Si. Light was set at 130 μmol photons m<sup>-2</sup> s<sup>-1</sup> and 16:8 light/dark cycles. A smaller culture was kept for more than ten generations with regular dilutions to allow acclimatization before Ti uptake, and incorporation experiments were performed on larger experimental cultures. The cultivation setup consisted of borosilicate culture vessels of cylindrical shape with conical ends, with a diameter of 8 cm and a height of 50 cm (approximately 1,500 mL working volume). The volume of the experimental cultures was 1.1–1.2 L. Silicone stoppers and silicone hoses were used to ventilate the cultures, which were placed in a growth cabinet at 20 °C. Pressurized air (provided by aquarium pumps) was used to mix the cultures, using a gentle stream of bubbles from the bottom of the culture vessels. Macronutrients NO<sub>3</sub>, PO<sub>4</sub> and Si were measured at selected time points during the acclimatization period to verify surplus (or in the case of Si, limitation before the experiments were initiated) using Merck Spectroquant test kits and SpectroquantPharo 100 spectrophotometer.

Instantaneous chlorophyll fluorescence ( $F_t$ ) and quantum yield ( $Q_y$ ) was monitored using a dual-mode AquaPen AP 100 (Photon Systems Instruments fluorometer) to assess the biomass changes and photophysiological condition of the cells during cultivation and experiments. *Pinnularia* sp. has a tendency to cluster, and cell counts can be biased. Therefore, the consumed Si and the  $F_t$  measurements were used to assess changes in the biomass.

## Ti uptake and incorporation experiments

Ti uptake experiments were initiated when the Si concentration in the medium was  $<0.5 \mu\text{mol L}^{-1}$  for two consecutive days and the cell numbers did not increase any further. Si limitation is known to induce cell cycle arrest in diatoms (Brzezinski et al. 1990), and the populations were expected to be highly synchronized at the start of the experiment. Visual inspection of samples at the start of the experiment showed some size differences, with cells of mainly three different sizes and with a mean cell size of  $35.2 \mu\text{m}$  (CV 8.2 %,  $n=67$ ). A large number of paired cells were observed, in accordance with the Si limitation and cell cycle arrest before the final cell separation. The experiment was performed two times. Pure crystalline  $\text{Ti}(\text{OH})_4$  was made according to Jeffryes et al. (2008), and a stock solution was prepared by dissolving the  $\text{Ti}(\text{OH})_4$  in concentrated HCl (37 wt.%) with continuous stirring on a hot plate ( $80^\circ\text{C}$ ). The stock solution was diluted with heated ( $80^\circ\text{C}$ ) deionised water to a final concentration of  $500 \text{ mM HCl}/0.36 \text{ mM Ti}$ . A solution of  $\text{Na}_2\text{SiO}_3 \cdot 9\text{H}_2\text{O}$  in  $500 \text{ mM NaOH}$  was made to balance the acidic Ti solution (final concentration  $6.2 \text{ mM Si}$ ), and the two solutions were added in equal volumes to the experimental cultures using two Cole-Parmer 94900 Syringe pumps. The total Si and Ti solution volume was added drop-wise over 10 h, and the pH was between 8.0 and 8.4 during the experiments.

Control experiments were performed with (a) only medium (without cells) and addition of approximately  $3.8 \mu\text{mol L}^{-1}$  Ti and  $160 \mu\text{mol L}^{-1}$  Si to verify that both Si and Ti are recovered with the medium and do not adsorb to the glassware and (b) a culture of *Pinnularia* sp. grown in plastic bottles to determine the background of Ti in frustules without the borosilicate glassware as a possible source of Ti.

After centrifuging to remove the culture medium, organic material was removed from the biosilica using SDS/EDTA ( $50 \text{ mg L}^{-1}$  in  $100 \text{ mM EDTA}$  solution), and the frustules were stored in methanol at  $-20^\circ\text{C}$  until analysed. One of the frustule samples from the Ti uptake experiments was chosen for determination of Ti by ICP-MS and analytical transmission electron microscopy (TEM). Control samples without addition of Ti were also analysed.

## Measurements of Ti by ICP-MS

High-resolution inductively coupled plasma mass spectrometry (HR ICP-MS; ELEMENT 2 instrument from Thermo Electronics) was used to determine the concentrations of Ti in seawater (background), cultivation medium and frustule samples, with and without incorporated Ti. A total of 2 mL of seawater or medium was filtered through  $0.2\text{-}\mu\text{m}$  syringe filters into 15-ml centrifuge tubes (metal-free, VWR collection) and conserved with  $\text{HNO}_3$  (1 g, ultrapure).

Samples were diluted  $10\times$  with deionised water before ICP-MS analysis. The reported measurements are the average of three technical replicates, with coefficient of variation (CV) of the mean (in %). In the medium samples, the CV was  $<5\%$  in all measurements.

Biosilica samples were rinsed with  $\text{HNO}_3$ , transferred to PF containers and dissolved in concentrated HF acid ( $0.18 \text{ mL}$ , grade supra pure). The dissolved frustules were diluted with  $0.1 \text{ M HNO}_3$  before ICP-MS analysis. The reported value is the average of two technical replicates, with CV 1.05 %.

The background value of Ti in *Pinnularia* frustules was determined from a culture grown in plastic bottles (to avoid any contribution from the glass material itself) but otherwise treated in the same way: The medium was the same as in the Ti uptake experiment (but no Ti was added), and the culture was aerated with pressurized air to promote mixing and gas transport. The background of Ti in seawater was determined from a sample of water collected from 80-m depth in the Trondheim fiord (the same water was used in the experiments).

## Analyses of Si and Ti by TEM

Transmission electron microscopy characterization was performed with two different instruments: (1) JEOL 2010 F operated at  $200 \text{ kV}$  and equipped with an  $80\text{-mm}^2$  silicon drift detector (SDD) for X-ray energy dispersive spectroscopy (EDS) and (2) double  $\text{C}_s$  corrected cold field emission gun JEOL JEM-ARM200F operated at  $200 \text{ kV}$ . This instrument is equipped with a large solid angle Centurio SDD and a Quantum GIF with a dual electron energy loss (EEL) spectrometer. This setup allows for simultaneous acquisition of a high-angle annular dark field (HAADF) scanning transmission electron microscopy (STEM) image in combination with energy dispersive spectroscopy (EDS) and two different EEL regions. Hence, in a spectrum image, an EDS spectrum and two different EEL spectra are acquired and quantified in every pixel of the image.

The TEM samples were prepared by dispersing the frustules on a holey, amorphous carbon-coated Cu TEM grid. A selection of 21 frustules from the first experiment was analysed (aiming at either a valve or the girdle band zone) by EDS in the JEOL 2010 F to determine the average Ti concentration. Three frustules with high average Ti concentration were then selected from the second experiment for further analysis using the JEM-ARM200F to map and quantify the Ti concentration with high spatial resolution. Each measurement is the average Ti concentration across a region with a diameter of 1 to  $2 \mu\text{m}$  (determined by the size/diameter of the electron beam) on the frustule, pointed at either valve or girdle band zones.

## Analysis of Si and Ti by X-ray photoelectron spectroscopy

Samples were also analysed by X-ray photoelectron spectroscopy (XPS) in order to determine the chemical state of the Ti at the surface and within the bulk of the frustules. A small drop of frustules in methanol was deposited on Al foil and dried. The analysis was performed using an Axis Ultra<sup>DLD</sup> XP spectrometer (Kratos Analytical) and monochromatic Al K $\alpha$  radiation. Pass energy of 160 eV was used for survey scans and 40-eV high-resolution scans of the individual core levels. Charge neutralization was applied, and the binding energy scale was referenced to the C 1 s component at 285 eV. The analysed area was approximately 300 $\times$ 700  $\mu\text{m}$ . Ion beam sputtering was used to remove surface materials and reveal the bulk composition for analysis. Sputtering was performed using 2-kV Ar ions, and the analysis area after sputtering was approximately 100  $\mu\text{m}$  in diameter.

## Results

### Growth and physiological status of *Pinnularia* sp

Under the environmental conditions provided here, the *Pinnularia* sp. cells maintained a specific growth rate of approximately 0.7 day<sup>-1</sup>, which corresponds to a doubling in cell numbers per day. Cell numbers counted at the start of the experiment was 4.11 $\times$ 10<sup>4</sup> cells mL<sup>-1</sup> (S.E.  $\pm$ 0.02,  $n$ =2). An average of 1.13 pmol Si cell<sup>-1</sup> was estimated from several measurements during the experiment ( $\pm$ 0.07, CV=5.87 %). A major fraction of the added Si was consumed during the first 24 h of the experiment or shortly after, corresponding to a biomass yield of approximately 4.20 $\times$ 10<sup>4</sup> new cells mL<sup>-1</sup>, i.e. a doubling in biomass within the experimental period.  $F_t$  measurements showed a doubling also in fluorescence and corroborated a twofold increase in biomass during the experiment.  $Q_Y$  is a measurement of the efficiency of conversion of absorbed light into photochemistry, and it is used to assess the photophysiological status of the cells.  $Q_Y$  was 0.42 at the beginning of the experiment, indicating that the cells were in a reasonably healthy photophysiological state despite the Si deprivation previous to the experimental starting time (data not shown). The  $Q_Y$  then decreased to 0.30 during the 10 h of Ti/Si addition and thereafter increased to 0.37 where it remained stable for 48 h. When there was less than 1  $\mu\text{mol Si L}^{-1}$  in the medium, the  $Q_Y$  sank to 0.25, indicating that the photophysiological condition was challenged.

### Dissolved Si and Ti in the cultures

A total of 48.6 $\pm$ 0.3 (SE,  $n$ =2)  $\mu\text{mol Si L}^{-1}$  of culture was added drop-wise to the experimental cultures during the first

10 h of the experiment, and 75 % of the added Si was removed from the medium by the cells during the first 24 h (Fig. 1). After 48 h, the dissolved Si (dSi) was low (1  $\mu\text{M}$ ), the biomass had ceased to increase and the experiment was terminated after 72 h. Simultaneously to the Si addition, 2.84 $\pm$ 0.01  $\mu\text{mol Ti L}^{-1}$  (SE,  $n$ =2) was added drop-wise to the experimental cultures. After 24 h, the medium contained only 0.086  $\mu\text{mol Ti L}^{-1}$  (i.e. 97 % was taken up; Fig. 1). The background of Ti in the seawater used was 0.0064  $\mu\text{M}$  ( $\pm$ 0.0001 SE,  $n$ =3) but somewhat higher in f/2 medium due to impurities in chemicals used to amend the seawater: 0.0094  $\mu\text{M}$  ( $\pm$ 0.0001 SE,  $n$ =3). A control experiment without algae enriched with approximately 3.8  $\mu\text{mol L}^{-1}$  Ti and 160  $\mu\text{mol L}^{-1}$  Si showed that both Si and Ti stayed in the solution after 24 and 48 h. The concentrations measured were somewhat lower than the added dose, but not more than 10 % and within the errors in analysis and dosage of Si and Ti added.

### Si and Ti in frustules

The ICP-MS analysis showed that a sample of frustules grown in plastic flasks with f/2 medium and no Ti added contained 0.001  $\mu\text{M Ti}$  (CV 17.7 %), which is comparable to the concentration of Ti observed in f/2 medium. A doubling of the biomass and concomitant removal of 2.76  $\mu\text{mol Ti L}^{-1}$  of culture within the first 24 h of the experiment indicated a cellular content of 33.2 fmol Ti per cell in the new cells or 2.37 wt.% Ti/SiO<sub>2</sub> (average over all frustules, not considering the difference between old and new valves, see the following related discussion). A low-resolution, bright-field TEM image (Fig. 2a) and a medium-resolution high-angle annular dark field (HAADF) scanning TEM (STEM) image (Fig. 2b) show the cleaned frustules with characteristic patterns of ribs and pores. The high-resolution HAADF STEM image of an area

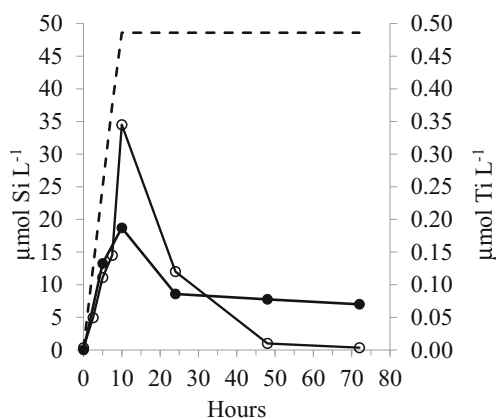
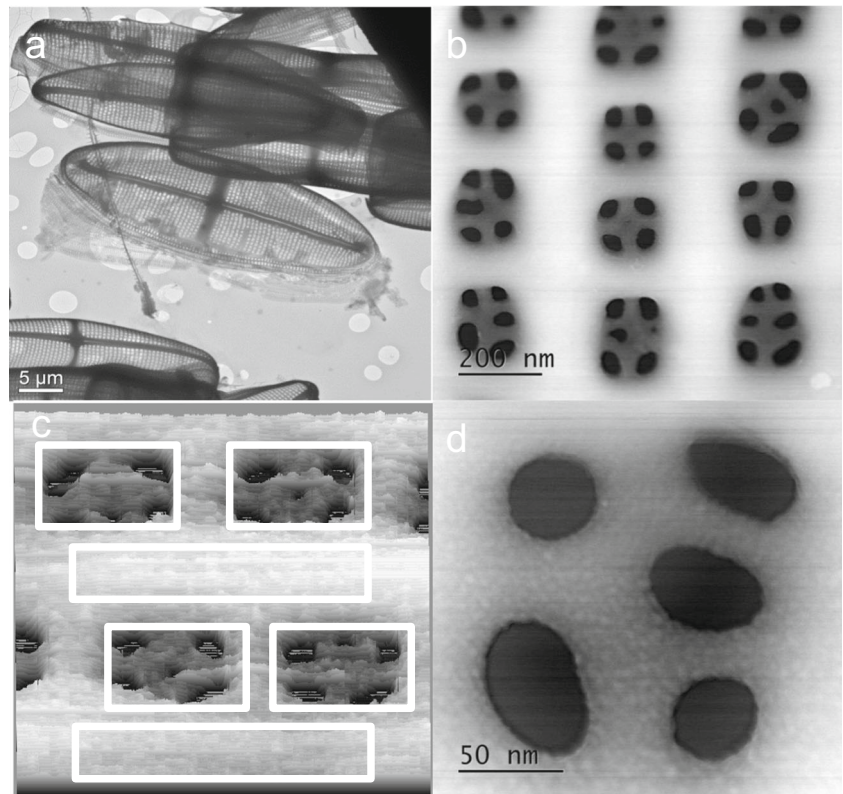


**Fig. 1** Dissolved Si ( $\mu\text{mol L}^{-1}$ , open circles) and dissolved Ti ( $\mu\text{mol L}^{-1}$ , filled circles) in the culture. The dotted line shows the addition of Si and Ti (calculated, not measured), which were added drop-wise for the first 10 h



**Fig. 2** **a** Low-resolution, bright-field TEM image of cleaned *Pinnularia* frustules from one of the Ti uptake experiments. **b** Section of a *Pinnularia* sp. valve with pores. **c** High annular dark field (HAADF) scanning transmission electron spectroscopy (STEM) image of an area which includes four pore openings and surrounding SiO<sub>2</sub>. The boxes indicate where EDS/EELS measurements were performed, and in the four pore areas the average Ti was 1.06 (±0.101) at.%. In the two areas between the pores, the Ti was 0.21 (±0.050) at.%. **d** High annular dark field (HAADF) scanning transmission electron spectroscopy (STEM) image of one of the pores showing the granular appearance of the amorphous SiO<sub>2</sub>



of pores revealed the granular surface of amorphous SiO<sub>2</sub>, with particles of 4 to 5 nm in diameter (Fig. 2d).

EDS analysis of 21 randomly selected frustules gave an average atomic O/Si ratio of 2.04±0.19 (SD), not significantly different from 2 (*p*=0.357). The EDS analysis showed Si contents of 29 to 37 at.%, with an average of 33 at.% (±2 SD). A quantile plot suggested good fit (assuming a normal distribution) for the Si content (linear relationship; Fig. 3a). Ti content was from 0 to 0.55 at.%, with an average of 0.23 at.% (±0.20 SD) over all the frustules. Based on a quantile plot, the Ti content showed a bi- or tri-phased relationship consistent with a model of old valves with low Ti content and new valves (synthesised during the experiment) with high Ti content

(Fig. 3a). The results also showed that there was an enrichment of Ti by a factor of 13 due to Ti addition: average Ti content of old valves was 0.023±0.017 at.%, compared to 0.300±0.148 at.% in new valves. The atomic ratios of Ti/Si in the 21 measurements were from 0 to 0.019 (Fig. 3b), and the distributions of Si and Ti were confirmed by Shapiro–Wilk test for normality with *p*=0.994 and *p*=0.009 for Si and Ti, respectively.

In order to provide finer detail about Ti distribution, three frustules with relatively high Ti concentrations were selected for high-spatial-resolution elemental mapping by simultaneous EDS and EELS. The EDS element maps from the three frustules showed significant differences between the Ti

**Fig. 3** **a** Quantile plot based on the assumption of normal distribution of elements in 21 cleaned valves from *Pinnularia* sp. The linear fit confirms normal distribution of Si (open circles). The distribution of Ti is bi- or tri-phasic and confirms the different quantities of Ti in old vs. new valves (filled circles). The distribution was tested using Shapiro–Wilks test for normality, and *p*=0.994 and 0.009 for Si and Ti, respectively. **b** Ti/Si ratios (atomic) in the 21 cleaned valves

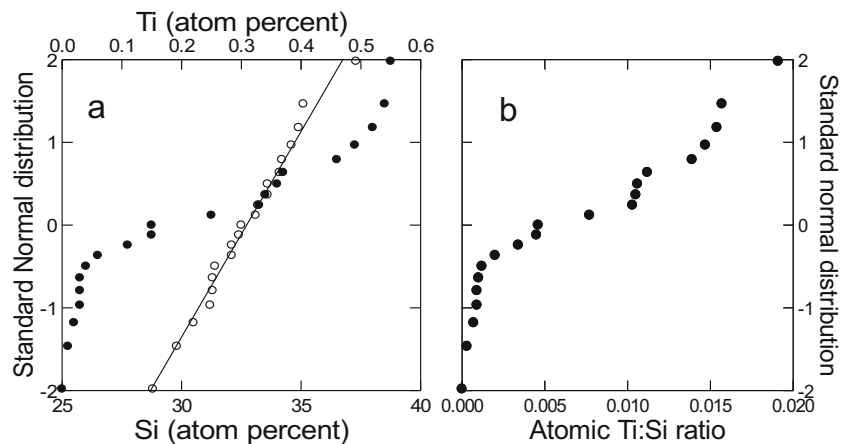


**Table 1** Oxygen, silicon and titanium (at.%) and ratio of Ti to Si measured by EDS in either pores or rib area on cleaned valves of *Pinnularia* sp. The values are average of measurements (with STD in parenthesis) from three frustules that showed high Ti content

	O	Si	Ti	Ti/Si	Number, <i>n</i>
Pores	67.8 (2.30)	31.2 (2.29)	1.06 (0.101)	0.034	10
Ribs	68.0 (1.62)	31.8 (1.56)	0.21 (0.050)	0.007	4

concentration in the pore linings and in the thicker SiO<sub>2</sub> regions between the pores (Fig. 2c). The Ti concentration in the thin pore lining regions was >1 at.%, i.e. five times more Ti than in the thicker regions between the pores (Table 1). EELS measurements confirmed the inhomogeneous distribution of Ti in the biosilica with 0.00 at.% Ti in the bulk SiO<sub>2</sub> (between pore areas) and 1.57 at.% Ti in the pore area/linings. The difference was evident also after correction for the variations in frustule thickness over the analysis area (Fig. 4). The energy loss spectra show the O K top around 540 eV present in both the pore region and the region between pores, while the Ti L2 and L3 tops (around 455–465 eV) are only present in the spectrum from the pore region (Fig. 5).

A XPS survey spectrum showed that, besides Si and O, C, N, Na and Ti were present as peaks that are associated with the surface of the frustules (Fig. 6a). The presence of Al and a proportion of the O signal are associated with the Al support foil. High-energy resolution scans from the Ti 2p peak region (Fig. 6b) before and after sputtering suggested the presence of Ti<sub>2</sub>O<sub>3</sub> or TiO in the valve (Ti 2p<sub>1/2</sub>~463 and Ti 2p<sub>3/2</sub>~457 eV); after sputtering, the Ti peaks were consistent with the presence of TiO<sub>2</sub> (Ti 2p<sub>1/2</sub>~464 and Ti 2p<sub>3/2</sub>~458 eV). The Si peak is consistent with the expected SiO<sub>2</sub> composition, Si 2p ~103 eV.

## Discussion

Bioincorporation of Si in combination with other elements such as Ti, Ge or Zn is considered as a means to modulate the material properties of diatom frustules for use in solar cell

technology. However, processes of element uptake and biosilicification must be understood in more detail before we are able to control the processes. Ti concentrations in the oceans are in the picomolar range, and natural marine phytoplankton contains up to 0.078 at.% Ti in the silica fraction (Martin and Knauer 1973). This is comparable to the lower amounts of Ti measured in the valves in our study (0.01–0.06 at.%), presumably the old valves that were produced prior to the Ti addition. The TEM images from this experiment show normally developed frustules without any obvious aberrations in the frustule shape or pore pattern, and thus growth in Ti-supplemented medium did not seem to interfere with the normal cell cycle and frustule synthesis. This was also supported by the measurements of fluorescence and quantum yield, which showed a doubling of the biomass and satisfactory photosynthetic performance during the first 24 h of the uptake experiment. From our measurements, the removal of Ti from the medium seemed to proceed with a rate proportional to that of Si, but how Ti is taken up or how fast it is taken up by the cells remains unknown. Based on the chemical similarities of Si(OH)<sub>4</sub> and Ti(OH)<sub>4</sub>, it is reasonable to assume that Ti is taken up via the same transport system as Si, but not necessarily in a constant or foreseeable ratio. Our study of Ti uptake and bioincorporation in *Pinnularia* sp. confirm that Ti is incorporated together with Si in the new frustules, in accordance with Jeffryes et al. (2008).

From our data, we see that there is a higher concentration of Ti around the pores on the valves (1.06 at.%), which is similar to the amounts and distribution patterns observed by Jeffryes et al. (2008). Our measurements include a correction for the uneven frustule thickness (Fig. 4) which Jeffryes et al. (2008) lacked, and the inhomogeneous distribution of Ti is therefore confirmed by our data. The fact that Ti is inhomogeneously distributed and concentrated around pores can be of use, for example, to enhance photon transport via the nano-scaled pores. If we understand why this happens, it would increase the possibility of biogenic manufacturing to produce frustules with special properties. Jeffryes et al. (2008) speculated that more Ti was deposited in the final stages of silica deposition due to Si pool exhaustion and slower rates of condensation of

**Fig. 4** EDS thickness map (left) used to correct the EELS Ti map for thickness variations over the valve and pores; the resulting 3D image (right) shows the increased amounts of Ti localized around the pore openings in the *Pinnularia* sp. valve

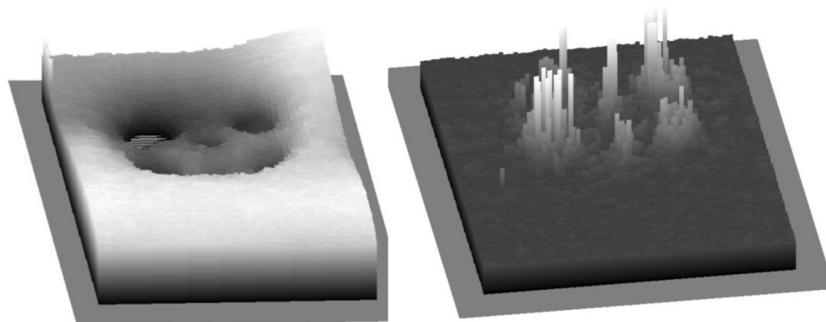
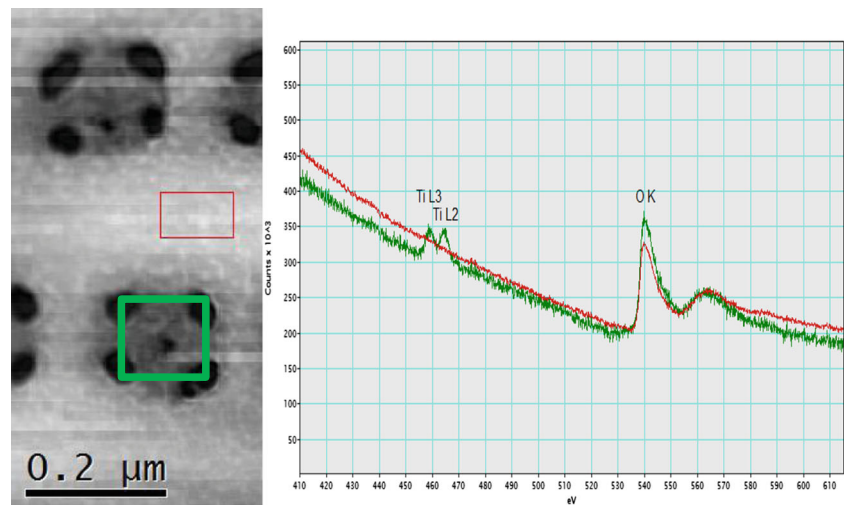


**Fig. 5** EELS data from pore region (green square and line) and between pores (red square and line) showing the O K peak around 540 eV present in both regions, while Ti L2 and Ti L3 (455–465 eV) are only observed in the spectra from the pore region

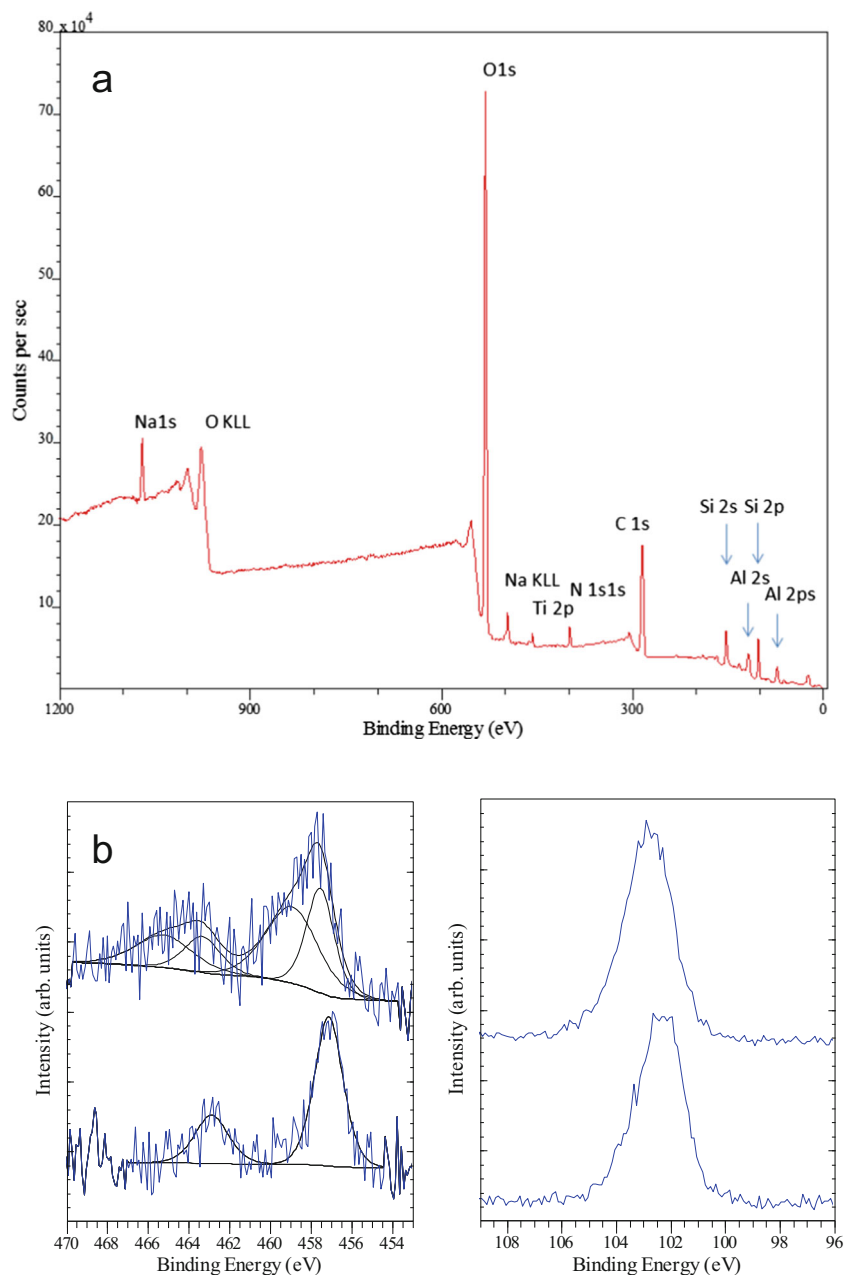


Ti to  $\text{TiO}_2$ . In our experiment, the first generation of cells produced with Ti enrichment were not Si-limited and the Si pools therefore presumably non-exhausted (Fig. 1). Ti and Si were available in the culture medium in an atomic ratio of 0.10 in the beginning of the experiment, and when the addition of Ti and Si stopped after 10 h, the ratio changed to 0.06. Using the removed Ti and Si to estimate the intracellular pools, it seems that the ratio was high and stable (0.17–0.19) during the 10 h of Ti and Si addition. This time frame is coincident with finalization of the frustule and cell separation into two individual daughter cells in the cells that were synchronized due to Si depletion and the beginning of frustule synthesis in the next generation of cells (and concomitantly active Si uptake). The ratio sank to 0.06–0.08 from 24 h, and the next generation would then have a lower intracellular pool at the time when they finalize the fine structures of the frustules. Another explanatory model that is not related to concentrations of Ti and Si during the frustule synthesis period is that the uneven distribution of Ti in the frustules may be caused by the chemical quality of micelles or moulding structures involved in silica deposition and pore construction during frustule synthesis. Synthesis of the new valves in raphid pennate diatoms such as *Pinnularia* sp. starts from the central raphe and then proceeds outwards with ribs and crossing connections that form pores (Sato et al. 2011; Cox et al. 2012), using the cytoskeleton actin microfilaments to direct the deposition. Silica is deposited in micro-fibrils radiating out from a mid-line and bi-directionally towards the valve surfaces, and the raphe opening and the areolar pores are lined afterwards with a thick layer of silica that is more resistant to alkaline etching (Crawford et al. 2009). The processes that lead to the differentiation between the micro-fibrillar silica construction and the thick lining around openings have not been revealed, but increased concentration of Ti in these lining areas may be connected to these processes. Also, fluidic phase-separation theories and mathematical modelling have been used to show

how the frustule architecture and pore pattern can arise by physio-chemical processes involving, e.g., polyamine micelles (Sumper 2002; Lenoci and Camp 2008; Willis et al. 2013), yet another explanatory model suggests that pores are constructed from molecular scaffolds or moulding structures onto which the Si is deposited or the scaffold creates an obstacle so that the Si deposition is interrupted at certain places, thus creating the pore patterns (Tesson and Hildebrand 2013). The exact composition of the scaffolds or moulding structures is not known, but chitin is found in close association with centric diatom valves and may play a role as a moulding agent (Brunner et al. 2009; Durkin et al. 2009).

The HAADF STEM image of a pore detail (Fig. 2d) revealed surface structures or particles of approximately 4 to 5 nm, which is very interesting considering that this is considerably smaller than the reported sizes of  $\text{SiO}_2$  precipitates made with natural diatom proteins. If the polymerization of Si occurs without salts or other ions present, colloidal particles of 2 to 3 nm in size are formed, and further development is dependent on pH and temperature (Coradin and Lopez 2003). Ions such as P, however, are known to influence the particle size of Si precipitates in vitro (Sumper et al. 2003), and Si particle size in frustules of living cells is also related to the different polyamines and proteins involved in Si precipitation (Kroger et al. 1999). A study by Lechner and Becker (2014) showed that different synthetic peptides resembling silaffins produced Si spheres of different sizes and also of different surface graininess depending on the numbers and positioning of lysine residues on the peptide. It is possible that we observed a grainy surface of larger Si polymers in the frustule surface. Also, Vertegel et al. (2004) demonstrated that the protein lysozyme adsorbed to Si nanoparticles of different sizes, and increasing particle size (40 or 100 nm) led to a higher degree of unfolding in the protein and concomitant decrease in activity. On small Si particles of 4 nm in diameter, however, the lysozyme did not unfold, and the activity was

**Fig. 6** **a** XPS analysis of cleaned *Pinnularia* sp. frustules on an Al foil showing the overall surface composition of the frustules after drying. **b** The effect of Ar ion sputtering on the Ti 2p (*left panel*) and Si 2p (*right panel*) peaks; the initial analysis is shown in the *lower curve*, and the *upper curve* shows the analysis of the same area after Ar ion sputtering. The peaks appear in the same energy regions as in **a** but with the signal acquired from a smaller area for more detail



higher. The relation between the proteins involved in biosilification and particle sizes is not fully understood, but a similar mechanism with small particles and enhanced protein activity could play a role also in frustule synthesis.

EDS analysis was used to analyse the amounts of Ti in the biosilica, and the distribution of  $\text{SiO}_2$  showed a good fit with the assumption of normal distribution. Ti, on the other hand, was distributed in a bi- or even tri-phasic pattern (Fig. 3), and this observation is related to the occurrence of valves from different times in the culture period. Some valves are old (mother valves from before Ti addition), and other valves are newly synthesised “daughters” with Ti incorporated in

the biosilica. The quantification of  $\text{TiO}_2$  around pores was considered approximate in the work of Jeffryes et al. (2008) due to scattering of the X-ray beam in the sample. In our measurements, higher spatial resolution was achieved by the application of EELS, and both EDS and EELS showed similar trends qualitatively with increased Ti around the pore linings and less Ti in the solid areas of biosilica between pores. The EELS measurements, however, indicated that the difference in Ti concentration from the pore regions to the regions between the pores is even larger than those quantified by EDS. This is because the EDS analysis suffered from stray radiation due to backscattered and diffracted electrons that hit other parts of the



sample than the region illuminated by the beam. EELS measurements, on the other hand, do not suffer from such stray signals.

The XPS analysis of valves from the Ti incorporation experiment verified the presence of TiO<sub>2</sub> in the bulk material of the valve before and after sputtering, and quantification of the peak areas gave a Ti/Si atomic ratio of ~0.05 (at). These results are consistent with the data from Lang et al. (2013) and Chrcanovic et al. (2012). High-energy resolution scans showed that the Si peak is consistent with the expected SiO<sub>2</sub> composition, also after sputtering. A component of the Ti 2p peak appears at higher binding energy, which is indicative of a higher oxidation state such as Ti<sub>2</sub>O<sub>3</sub>/Ti<sup>3+</sup> (Fig. 6b). There was a slight shift of 0.5–1 eV compared to the peaks measured before sputtering, but we cannot say with certainty from our data that the valve surface contains Ti<sub>2</sub>O<sub>3</sub> or TiO. These results are difficult to interpret unambiguously due to charge compensation effects and the influence of the ion beam on the surface chemistry. The analysis is consistent with the presence of Ti<sup>3+</sup> in the frustules, allowing for some uncertainty due to damage caused by the ion beam. The energy shift between oxidised and metallic Ti, however, is ~5 eV, and allowing for the uncertainty in energy reference, it is regarded as large enough to eliminate the possibility of a metallic component in the spectra. Mayer et al. (1995) described the influence of ion damage on the XPS spectrum obtained from TiO<sub>2</sub> thin films. There are few studies of the biochemistry of Ti in cells or frustules (Buettner and Valentine 2012), but different Ti oxidation states in the frustule surface layers may be a result of the biochemical processes leading to the incorporation of Ti in the SiO<sub>2</sub> or post-incorporation chemical modifications due to, e.g., cleaning with SDS, sample storage or exposure to air during the analyses. The presence of other elements such as C, N or Na can be related to remnants of organic molecules that were involved in the frustule synthesis (e.g. N-rich polyamines) and therefore tightly integrated into the SiO<sub>2</sub>. The SDS cleaning used here is considered a mild cleaning process that does not remove completely all the organic components of the valve. It is also possible that the organic remnants stem from other sources, and for example, adsorption of hydrocarbon or carbon oxygen species from the air onto the Ti surface of dental implants is known (Chrcanovic et al. 2012).

Our data confirm the uptake and incorporation of Ti into diatom nanostructures, and a relatively high doping effect is achieved in the pore lining areas. The inhomogeneous distribution of the element influences the application of Ti-doped frustules in, e.g., solar cell technology, and how this effect can be exploited needs more investigations into the material technological properties.

**Acknowledgments** This work is part of the project “SOLBIOPTA-Biotechnological Production of Materials for Optimized Solar Cell Efficiency” that received funding from the Norwegian Research Council

(project no. 200013). We thank Syverin Lierhagen at Department of Chemistry/NTNU for help with the ICP-MS analyses.

**Open Access** This article is distributed under the terms of the Creative Commons Attribution License which permits any use, distribution, and reproduction in any medium, provided the original author(s) and the source are credited.

## References

- Annenkov VV, Basharina TN, Danilovtseva EN, Grachev MA (2013) Putative silicon transport vesicles in the cytoplasm of the diatom *Synedraacus* during surge uptake of silicon. *Protoplasma* 250:1147–1155
- Aw MS, Simovic S, Yu Y, Addai-Mensah J, Losic D (2012) Porous silica microshells from diatoms as biocarrier for drug delivery applications. *Powder Technol* 223:52–58
- Basharina TN, Danilovtseva EN, Zelinskiy SN, Klimenkov IV, Likhoshway YV, Annenkov VV (2012) The effect of titanium, zirconium and tin on the growth of diatom *Synedraacus* and morphology of its silica valves. *Silicon* 4:239–249
- Brunner E, Groeger C, Lutz K, Richthammer P, Spinde K, Sumper M (2009) Analytical studies of silica biomineralization: towards an understanding of silica processing by diatoms. *Appl Microbiol Biotechnol* 84:607–616
- Brzezinski MA, Olson RJ, Chisholm SW (1990) Silicon availability and cell-cycle progression in marine diatoms. *Mar Ecol Prog Ser* 67:83–96
- Buettner KM, Valentine AM (2012) Bioinorganic chemistry of titanium. *Chem Rev* 112:1863–1881
- Chrcanovic BR, Pedrosa AR, Martins MD (2012) Chemical and topographic analysis of treated surfaces of five different commercial dental titanium implants. *Mater Res* 15:372–382
- Cole KE, Ortiz AN, Schoonen MA, Valentine AM (2006) Peptide- and long-chain polyamine-induced synthesis of micro- and nanostructured titanium phosphate and protein encapsulation. *Chem Mater* 18:4592–4599
- Coradin T, Lopez PJ (2003) Biogenic silica patterning: simple chemistry or subtle biology? *ChemBiochem* 4:251–259
- Cox EJ, Willis L, Bentley K (2012) Integrated simulation with experimentation is a powerful tool for understanding diatom valve morphogenesis. *Biosystems* 109:450–459
- Crawford SA, Chiovitti A, Pickett-Heaps J, Wetherbee R (2009) Micromorphogenesis during diatom wall formation produces siliceous nanostructures with different properties. *J Phycol* 45:1353–1362
- De Stefano L, Maddalena P, Moretti L, Rea I, Rendina I, De Tommasi E, Mocella V, De Stefano M (2009) Nano-biosilica from marine diatoms: a brand new material for photonic applications. *Superlattice Microst* 46:84–89
- Del Amo Y, Brzezinski MA (1999) The chemical form of dissolved Si taken up by marine diatoms. *J Phycol* 35:1162–1170
- Durkin CA, Mock T, Armbrust EV (2009) Chitin in diatoms and its association with the cell wall. *Eukaryot Cell* 8:1038–1050
- Gale DK, Jeffryes C, Gutu T, Jiao J, Chang C-h, Rorrer GL (2011) Thermal annealing activates amplified photoluminescence of germanium metabolically doped in diatom biosilica. *J Mater Chem* 21:10658–10665
- He J, Chen D, Li Y, Shao J, Xie J, Sun Y, Yan Z, Wang J (2013) Diatom-templated TiO<sub>2</sub> with enhanced photocatalytic activity: biomimetics of photonic crystals. *Appl Phys A: Mater Sci Process* 113:327–332
- Hildebrand M (2008) Diatoms, biomineralization processes, and genomics. *Chem Rev* 108:4855–4874
- Jeffryes C, Gutu T, Jiao J, Rorrer GL (2008) Metabolic insertion of nanostructured TiO<sub>2</sub> into the patterned biosilica of the diatom

- Pinnularia* sp by a two-stage bioreactor cultivation process. ACS Nano 2(10):2103–2112
- Jeffries C, Campbell J, Li H, Jiao J, Rorrer G (2011) The potential of diatom nanobiotechnology for applications in solar cells, batteries, and electroluminescent devices. Energy Environ Sci 4:3930–3941
- Kinrade SD, Gillson AME, Knight CTG (2002) Silicon-29 NMR evidence of a transient hexavalent silicon complex in the diatom *Naviculapellucida*. J Chem Soc Dalton Trans 3:307–309
- Kroger N, Deutzmann R, Sumper M (1999) Polycationic peptides from diatom biosilica that direct silica nanosphere formation. Science 286:1129–1132
- Kroger N, Dickerson MB, Ahmad G, Cai Y, Haluska MS, Sandhage KH, Poulsen N, Sheppard VC (2006) Bioenabled synthesis of rutile (TiO<sub>2</sub>) at ambient temperature and neutral pH. Angew Chem Int Ed 45:7239–7243
- Lang Y, del Monte F, Rodriguez BJ, Dockery P, Finn DP, Pandit A (2013) Integration of TiO<sub>2</sub> into the diatom *Thalassiosira weissflogii* during frustule synthesis. Sci Rep 3
- Lechner CC, Becker CFW (2014) A sequence–function analysis of the silica precipitating silaffin R5 peptide. J Pept Sci 20:152–158
- Lenoci L, Camp PJ (2008) Diatom structures templated by phase-separated fluids. Langmuir 24:217–223
- Li N, Sioutas C, Cho A, Schmitz D, Misra C, Sempf J, Wang MY, Oberley T, Froines J, Nel A (2003) Ultrafine particulate pollutants induce oxidative stress and mitochondrial damage. Environ Health Perspect 111:455–460
- Mao L, Liu J, Zhu S, Zhang D, Chen Z, Chen C (2014) Sonochemical fabrication of mesoporous TiO<sub>2</sub> inside diatom frustules for photocatalyst. Ultrason Sonochem 21:527–534
- Martin JH, Knauer GA (1973) Elemental composition of plankton. Geochim Cosmochim Acta 37:1639–1653
- Mayer JT, Diebold U, Madey TE, Garfunkel E (1995) Titanium and reduced titania overlayers on titanium dioxide (110). J Electron Spectrosc Relat Phenom 73:1–11
- Miller RJ, Bennett S, Keller AA, Pease S, Lenihan HS (2012) TiO<sub>2</sub> nanoparticles are phototoxic to marine phytoplankton. PLoS ONE 7(1)
- Mock T, Samanta MP, Iverson V, Berthiaume C, Robison M, Holtermann K, Durkin C, BonDurant SS, Richmond K, Rodesch M, Kallas T, Huttlin EL, Cerrina F, Sussmann MR, Armbrust EV (2008) Whole-genome expression profiling of the marine diatom *Thalassiosira pseudonana* identifies genes involved in silicon bioprocesses. Proc Natl Acad Sci U S A 105:1579–1584
- Sato S, Watanabe T, Nagumo T, Tanaka J (2011) Valve morphogenesis in an araphid diatom *Rhaphoneisamphiceros* (Rhaphoneidaceae, Bacillariophyta). Phycol Res 59:236–243
- Sclafani M, Juffmann T, Knobloch C, Arndt M (2013) Quantum coherent propagation of complex molecules through the frustule of the alga *Amphipleurapellucida*. New J Phys 15
- Shea R, Chopin T (2007) Effects of germanium dioxide, an inhibitor of diatom growth, on the microscopic laboratory cultivation stage of the kelp, *Laminariasaccharina*. J Appl Phycol 19:27–32
- Spinde K, Pachis K, Antonakaki I, Paasch S, Brunner E, Demadis KD (2011) Influence of polyamines and related macromolecules on silicic acid polycondensation: relevance to “soluble silicon pools”? Chem Mater 23:4676–4687
- Sumerel JL, Yang WJ, Kisailus D, Weaver JC, Choi JH, Morse DE (2003) Biocatalytically templated synthesis of titanium dioxide. Chem Mater 15:4804–4809
- Sumper M (2002) A phase separation model for the nanopatterning of diatom biosilica. Science 295:2430–2433
- Sumper M, Lorenz S, Brunner E (2003) Biomimetic control of size in the polyamine-directed formation of silica nanospheres. Angew Chem Int Ed 42:5192–5195
- Tesson B, Hildebrand M (2013) Characterization and localization of insoluble organic matrices associated with diatom cell walls: insight into their roles during cell wall formation. PLoS ONE 8(4)
- Thamatrakoln K, Hildebrand M (2007) Analysis of *Thalassiosira pseudonana* silicon transporters indicates distinct regulatory levels and transport activity through the cell cycle. Eukaryot Cell 6:271–279
- Toster J, Iyer KS, Xiang W, Rosei F, Spiccia L, Raston CL (2013) Diatom frustules as light traps enhance DSSC efficiency. Nanoscale 5:873–876
- Vertegel AA, Siegel RW, Dordick JS (2004) Silica nanoparticle size influences the structure and enzymatic activity of adsorbed lysozyme. Langmuir 20:6800–6807
- Willis L, Cox EJ, Duke T (2013) A simple probabilistic model of submicroscopic diatom morphogenesis. J Roy Soc Interface 10(83)
- Yamanaka S, Yano R, Usami H, Hayashida N, Ohguchi M, Takeda H, Yoshino K (2008) Optical properties of diatom silica frustule with special reference to blue light. J Appl Phys 103(7)
- Zurzolo C, Bowler C (2001) Exploring bioinorganic pattern formation in diatoms. A story of polarized trafficking. Plant Physiol 127:1339–1345